Supplementary Information

Facile in situ synthesis of silver nanoclusters for promoting highly sensitive surface-enhanced Raman scattering detection of alkyne-tagged biomolecules

Leixin Hou,[a]* Mi Zhang,[a] Daofu Liu,[a] Mai Xu[a] and Huilin Huang[b]*

[a] School of Chemistry and Materials Engineering, Huainan Normal University, Huainan, Anhui, 232000, P. R. China

[b] School of Chemical and Printing Dyeing Engineering, Henan University of Engineering, Zhengzhou, 451191, P. R. China

Corresponding Authors

* E-mail: houleixin@hnnu.edu.cn, huangxiaoya1992@mail.dlut.edu.cn

Contents

1. General Materials and Methods
2. Experimental Section
3. Characterization of TOS-Ag_4 NCs and TNS-Ag_8 NCs
4. SERS measurements of TOS-Ag_4 NCs and TNS-Ag_8 NCs
5. References

1. General Materials and Methods

All starting chemicals and reagents were commercially available and used without further purification unless specifically mentioned. Powder X-ray diffraction (PXRD) measurements were obtained on a Rigaku Smart Lab XRD instrument with a sealed Cu tube (λ = 1.54178 Å). Thermogravimetric (TG) analyses were performed from 20 to 700 ℃ at a heating rate of 10 ℃ min^{-1} and a N_2 flow rate of 50 mL min^{-1}. Fourier transform infrared (FT-IR) spectra were collected in the range of 400-3500 cm^{-1} as KBr pellets on Thermo Fisher-6700. Raman spectra were collected on a Lab Raman HR Evolution at excitation wavelength of 633 nm in a scan range from 500 to 3500 cm^{-1} on powdered samples on air. Nitrogen sorption isotherms were recorded on a Quantachrome Autosorb-iQ at 77 K within a pressure range from P/P_0 = 0.001-0.99. The specific surface areas were evaluated by the Brunauer-Emmett-Teller (BET) method. Scanning electron microscopy (SEM) images were recorded with an HITACHI UHR FE-SEM SU8220 scanning electron microscope equipped with a field emission gun operated at 3-5 kV. The solid UV-vis spectra were recorded on a Hitachi U-4100 UV-vis-NIR spectrophotometer. X-ray photoelectron spectroscopy (XPS) was measured using Thermo ESCALAB-250XI. ^{1}H NMR spectra were recorded in the designated solvents on Varian DLG 400 M spectrometer with chemical shift in ppm.

2. Experimental Section

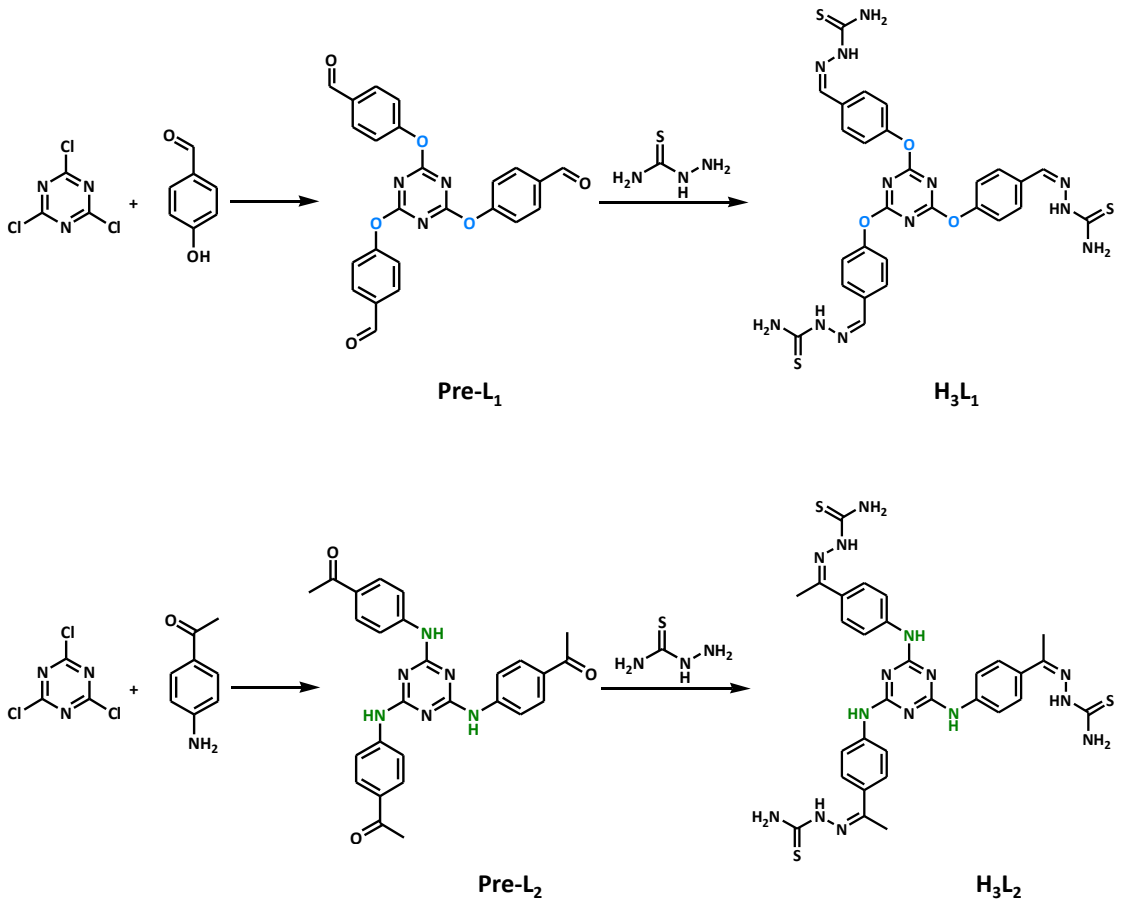

Scheme S1. Synthesis route of ligands H_3L_1 and H_3L_2.

Synthesis of H_3L_1 (2,2',2''-((((1,3,5-Triazine-2,4,6-triyl)tris-(oxy))tris(benzene-4,1-diyl))tris(methanylylidene))tris (hydrazinecarbothioamide)).

2,4,6-Tris(4-formyl phenoxy)-1,3,5-triazine (**pre-L_1**) was synthesized following a modified literature procedure.[S1] Acetic acid (0.5 mL) was added portionwise over 10 min to a mixture of **pre-L_1** (0.88 g, 2 mmol) and thiosemicarbazide (0.56 g, 6.2 mmol) in dry ethyl alcohol (50 mL). The resulting mixture stirred at refluxing for overnight. After cooling to room temperature, the pale yellow precipitate was filtered. Then the precipitate washed with ethanol (3 × 10 mL) and diethyl ether (3 × 10 mL) to get the **H_3L_1** as a pale yellow powder. Yield: 85%.

^{1}H NMR [400 MHz, DMSO-d_6, ppm]: 11.46 (s, 1H, CH), 8.21 (s, 1H, -NH), 8.04 (s, 2H, -NH2), 7.88 (d, 2H, Ar-H), 7.31 (d, 2H, Ar-H).

Synthesis of H_3L_2 (2,2′,2″-((((1,3,5-Triazine-2,4,6-triyl)tris- (azanedidiyl))tris(benzene-4,1-diyl))tris(ethan-1-yl-1-ylidene))tris(hydrazine carbothioamide)).

2,4,6-Tris(4-acetylphenylamino)-1,3,5- triazine (**pre-L_2**) was synthesized following a modified literature procedure.[S2] A mixture of **pre-L_2** (0.96 g, 2 mmol) and thiosemicarbazide (0.6 g, 6.6 mmol) in 50 mL of acetic acid was refluxed overnight. After cooling to room temperature, the yellow precipitate was filtered. Then the precipitate washed with ethanol (3 × 10 mL) and diethyl ether (3 × 10 mL) to get the **H_3L_2** as a yellow powder. Yield: 90%.

^{1}H NMR [400 MHz, DMSO-d_6, ppm]: 10.16 (s, 1H, -NH), 9.58 (s, 1H, Ar-NH-), 8.26 (s, 1H, -NH_2), 7.93-7.84 (m, 5H, Ar-H and -NH_2).

Synthesis of TOS-Ag_4 NCs

In a 200 mL glass flask, **H_3L_1** (262.4 mg) was dissolved in DMF (40 mL), and heated to 40 ℃ using oil bath. **$AgCF_3COO$** (265 mg) in 40 mL CH_3CN was carefully drops added to the H_3L_1/DMF solution under the rapid stirring condition for 60 min. After complete addition, the precipitate washed with ethanol (3 × 20 mL) and diethyl ether (3 × 20 mL) to get the **TOS-Ag_4 NCs** as a pale yellow powder. Yield: 55%.

Synthesis of TNS-Ag_8 NCs

In a 200 mL glass flask, **H_3L_2** (280.3 mg) was dissolved in DMF (40 mL), and heated to 40 ℃ using oil bath. **$AgBF_4$** (233 mg) in 20 mL CH_3CN was carefully drops added to the H_3L_2/DMF solution under the rapid stirring condition for 60 min. After complete addition, the precipitate washed with ethanol (3 × 20 mL) and diethyl ether (3 × 20 mL) to get the **TNS-Ag_8 NCs** as a pale yellow powder. Yield: 65%.

SERS measurements

In the SERS experiments, the soaking method was selected, and rhodamine 6G (R6G) molecules was used as the probe molecule. Both silver-based nanoclusters substrates were respectively immersed into 6 mL of different concentrations of R6G ethanol solutions (10^{-1} ~10^{-8} M) for over 30 min, followed by rinsing with ethanol and drying at room temperature. For the Alkyne-Tagged Biomolecules target experiments, similar to the above experiment process, the prepared both silver-based nanoclusters

substrate were repeatedly dipped into 6 mL 5-ethynyl-2′-deoxyuridine (EdU) or erlotinib (ETB) ethanol solutions with different concentrations for SERS measurements. The SERS Raman detection was carried out on a Dilor confocal laser Raman system with a 5 mW He-Ne laser at 633 nm. The integration time was 5 s with three accumulations.

Enhancement Factor (EF) Calculation of R6G/Alkyne-Tagged Biomolecules on the surface of TOS-Ag_4 NCs and TNS-Ag_8 NCs

To quantify the enhancement contribution of the TOS-Ag_4 NCs and TNS-Ag_8 NCs, we calculated their average SERS enhancement factor (EF) based on the following expression:

$$\mathrm{EF} = (I_{SERS}/N_{SERS})/(I_{NR}/N_{NR}) = I_{SERS}N_{NR}/I_{NR}N_{SERS}$$

where I_{SERS} stands for the intensities of the vibrational mode in the SERS spectra and I_{NR} stands for the normal Raman spectra of solid R6G/Alkyne-Tagged Biomolecules. N_{SERS} and N_{NR} are the number of R6G molecules/Alkyne-Tagged Biomolecules adsorbed on the SERS substrate and bulk molecules illuminated by the laser focus spot under SERS and normal Raman conditions, respectively. I_{SERS} and I_{NR} can be obtained from the spectra directly while N_{SERS} and N_{NR} need to be calculated on the basis of the estimation of the corresponding sample area. N_{SERS} and N_{NR} can be obtained according to the reported method.[S3, S4]

Suppose the target molecules uniformly dispersed on the substrate and then the density of the molecules on the substrate was assumed to be 1.0×10^{-6} mol/L × 20 μL × N_A /7.0 mm^2 (the surface area of the substrate is 7.0 mm^2). The laser spot has a 1μm diameter and the surface area is about 7.8×10^{-7} mm^2, so N_{SERS} value is estimated as following:

$$N_{\mathrm{SERS}} = 4.0 \times 10^{-6}\ \mathrm{mol/L} \times 10 \times 10^{-6}\ \mathrm{L} \times \mathrm{N_A} \times (7.8 \times 10^{-7}/7.0) = 1.34 \times 10^{6}$$

Taking the laser spot diameter (about 1 μm), the penetration depth (about 2 μm), and the molecule weight of solid R6G (1.26 g/cm^3) into account, N_{NR} had a value of 2.6×10^9 in the detected solid sample area.

3. Characterization of TOS-Ag_4 NCs and TNS-Ag_8 NCs

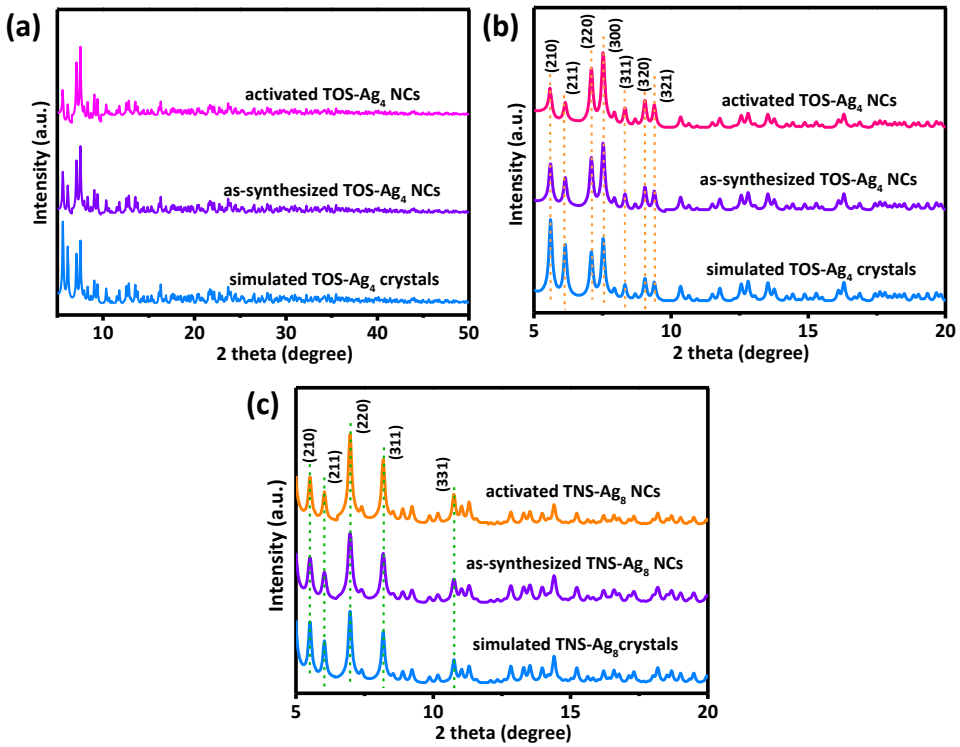

Figure S1. (a) PXRD patterns of the simulated TOS-Ag_4 crystals, as-synthesized and acetone activated TOS-Ag_4 NCs. (b) XRD fine scanning patterns of the simulated TOS-Ag_4 crystals, as-synthesized and acetone activated TOS-Ag_4 NCs. (c) XRD fine scanning patterns of the simulated TNS-Ag_8 crystals, as-synthesized and acetone activated TNS-Ag_8 NCs.

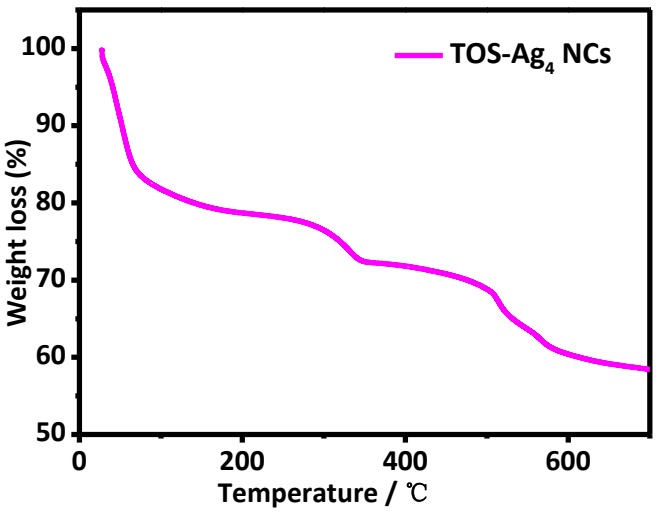

Figure S2. TGA curves of activated TOS-Ag_4 NCs samples.

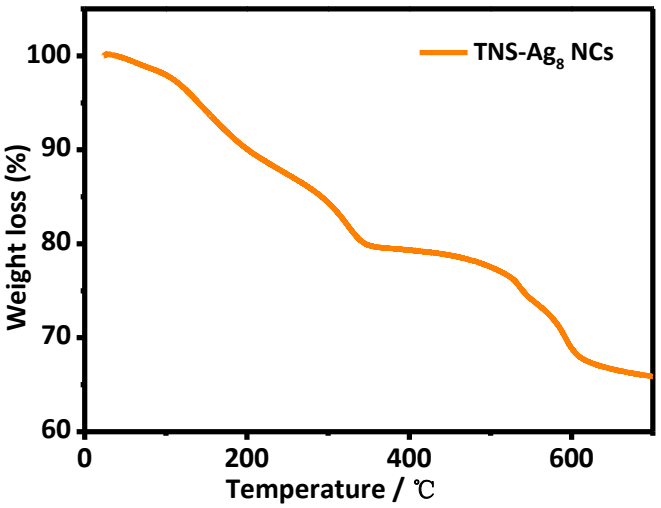

Figure S3. TGA curves of activated TNS-Ag_8 NCs samples.

Dye Uptake Method: Before the dye uptake experiments, TOS-Ag_4 NCs and TNS-Ag_8 NCs were firstly washed with acetone three times for guest molecular exchange. Then, the TOS-Ag_4 NCs and TNS-Ag_8 NCs were soaked in a methanol solution of 2,7'-dichlorofluorescein on oscillator overnight at room temperature. The resulting nanoclusters were washed with methanol thoroughly to remove the residual dye from the nanoclusters surfaces until the solution become colourless, and then dried under a stream of air. The dried-out nanoclusters (X mg) were dissociated by concentrated hydrochloric acid (2ml), and the solution was diluted to 3ml with DMF. Absorption experiments were performed on a UV-vis spectrophotometer. The concentration of 2,7'-dichlorofluorescein dye (Y mg/L) was determined by comparing UV-vis absorption with the standard curve (Figure S4).

Table S1. The results of 2,7'-dichlorofluorescein dye uptake.

	TOS-Ag_4 NCs	**TOS-Ag_4 crystals**	**TNS-Ag_8 NCs**	**TNS-Ag_8 crystals**
Sample + dye (X mg)	3.5	3.9	3.8	4.2
Dye concentration (Y mg/L)	79.3	71.6	82.3	76.5
The ratio of dye uptake (w/w)	12.7 %	10.1 %	12.1 %	10.0 %

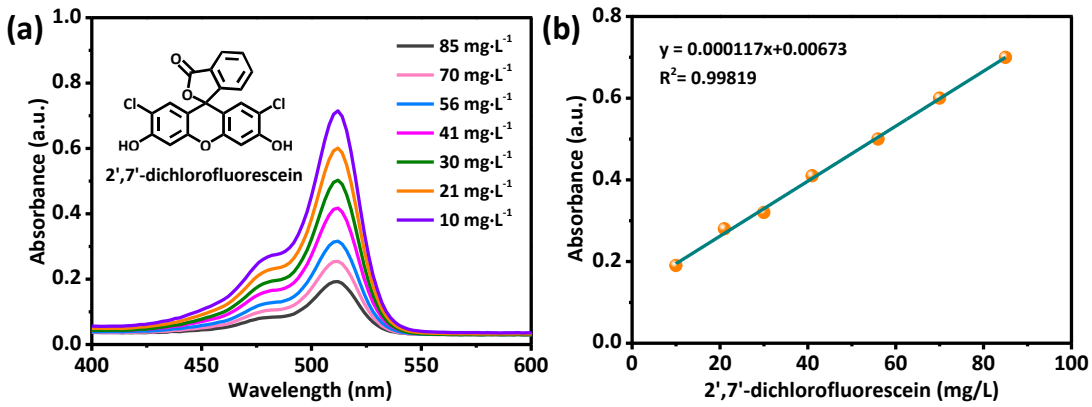

Figure S4. (a) UV-vis spectrum of different concentration of 2, 7'-dichlorofluorescein dye. (b) The standard linear relationship between the absorption and concentration.

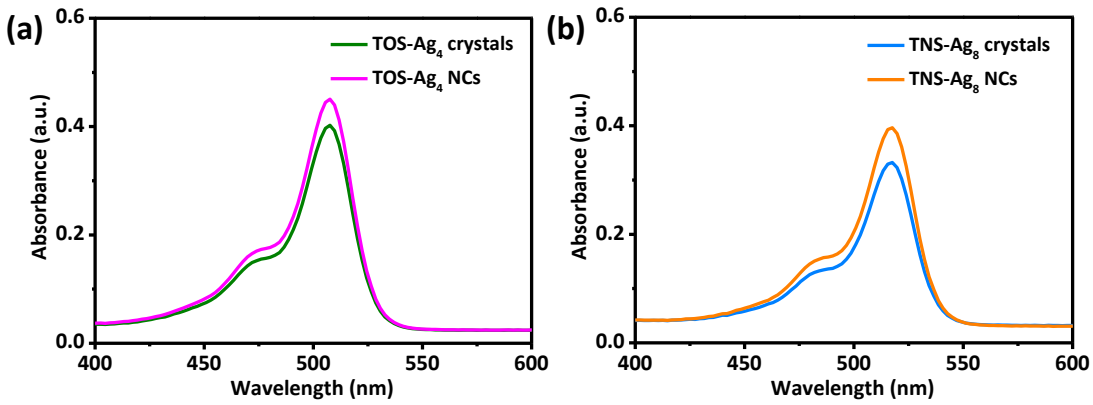

Figure S5. (a) UV-vis spectrum of different concentration of 2,7'-dichlorofluorescein dye. (b) The standard linear relationship between the absorption and concentration.

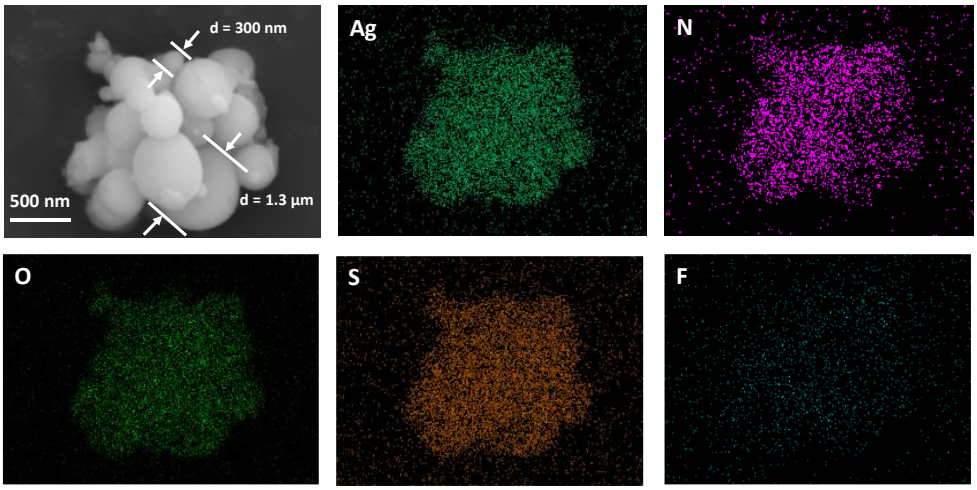

Figure S6. SEM and the EDS mapping images of TOS-Ag_4 NCs.

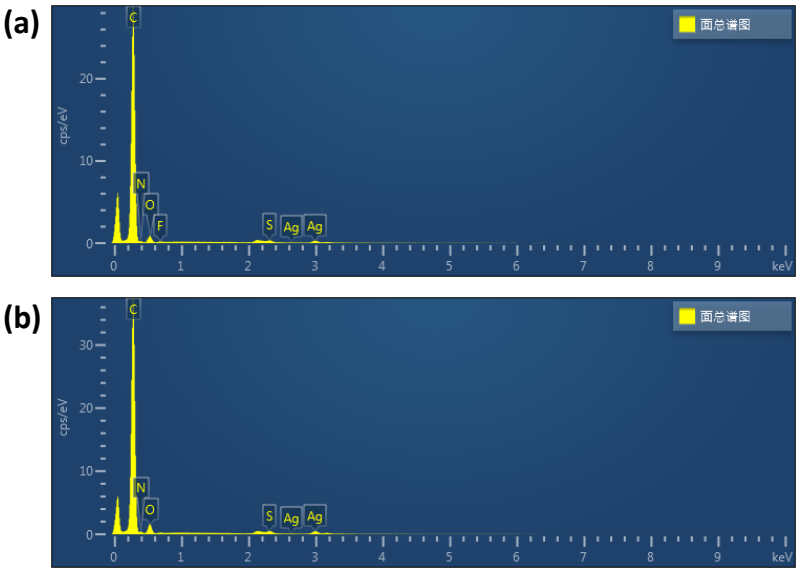

Figure S7. The EDS spectra of (a) TOS-Ag_4 NCs and (b) TNS-Ag_8 NCs.

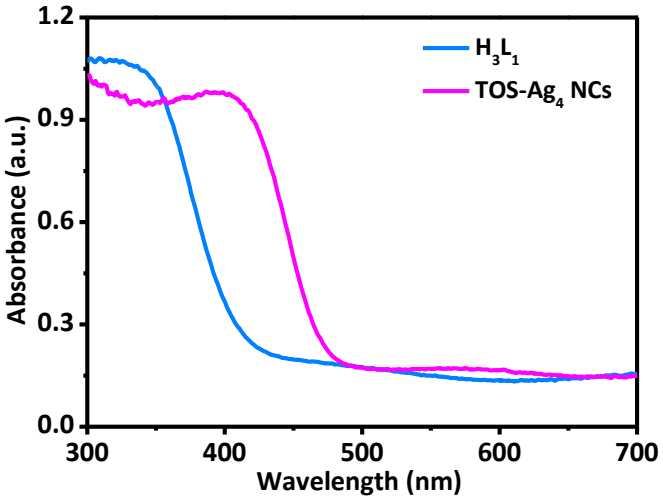

Figure S8. The solid-phase UV-vis spectra of TOS-Ag_4 NCs and its ligand H_3L_1.

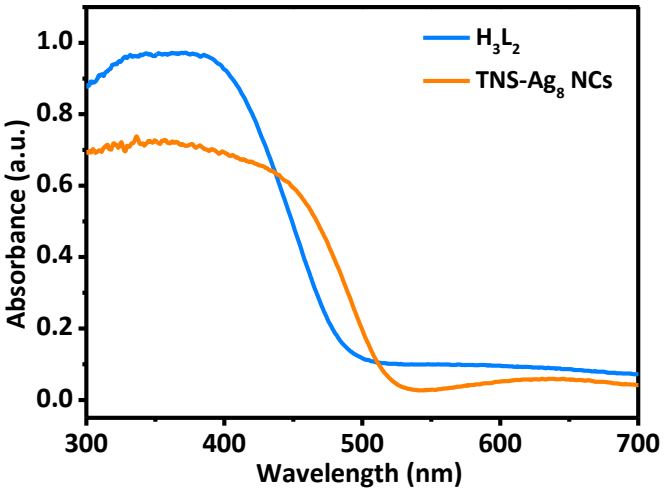

Figure S9. The solid-phase UV-vis spectra of TNS-Ag_8 NCs and its ligand H_3L_2.

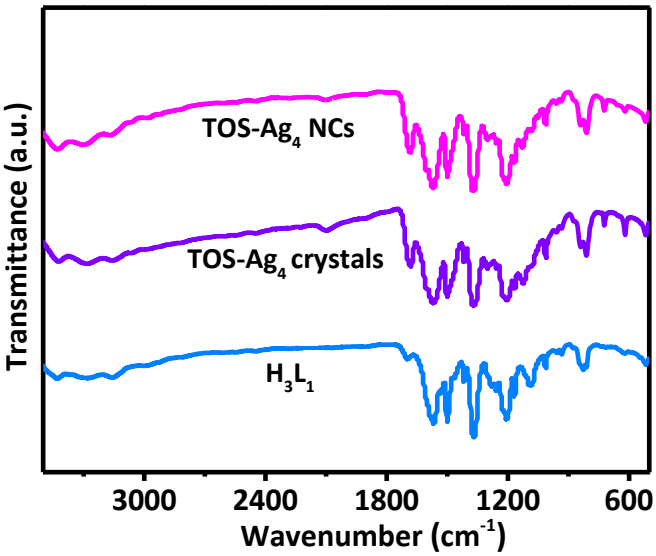

Figure S10. The Diffuse Reflectance FT-IR of H_3L_1, TOS-Ag_4 crystals and TOS-Ag_4 NCs.

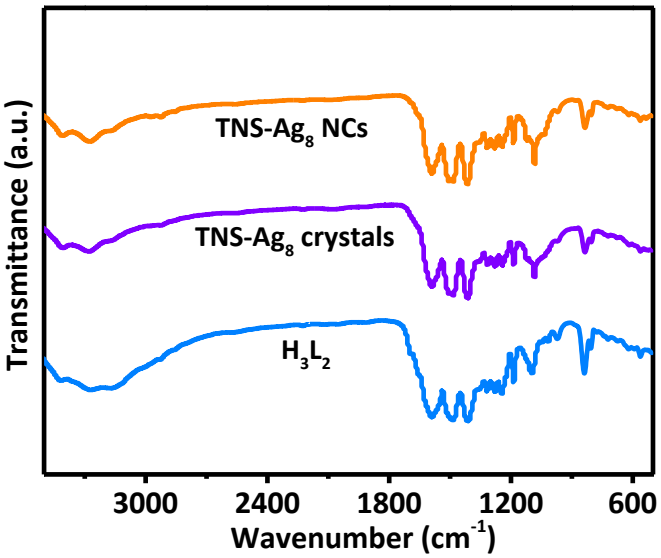

Figure S11. The Diffuse Reflectance FT-IR of H_3L_2, TNS-Ag_8 crystals and TNS-Ag_8 NCs.

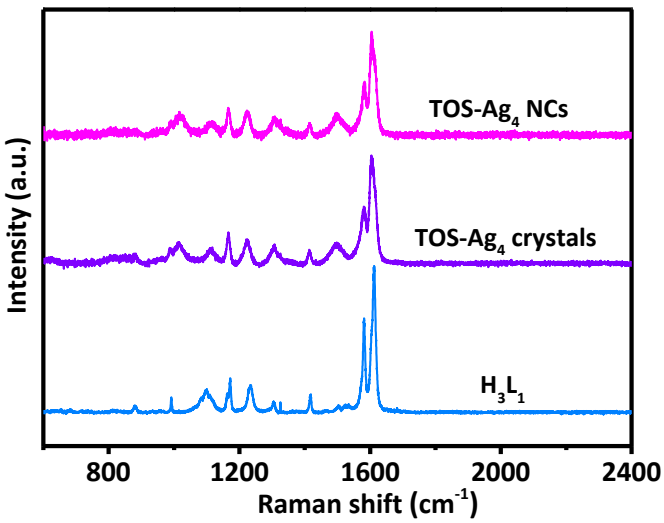

Figure S12. The laser Raman confocal microspectrometry of H_3L_1, TOS-Ag_4 crystals and TOS-Ag_4 NCs.

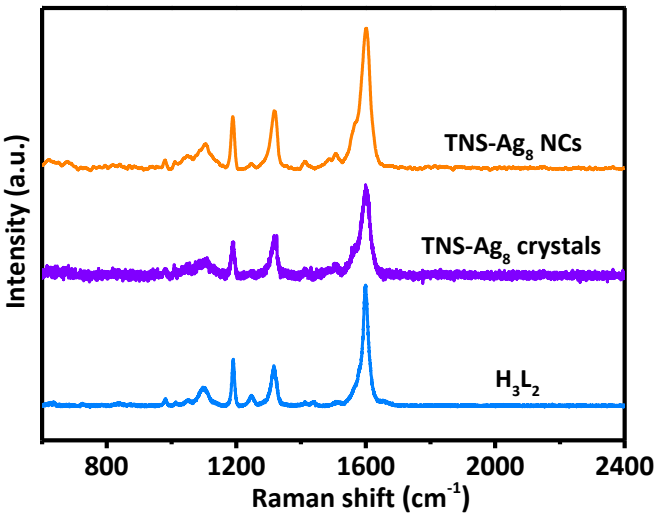

Figure S13. The laser Raman confocal microspectrometry of H_3L_2, TNS-Ag_8 crystals and TNS-Ag_8 NCs.

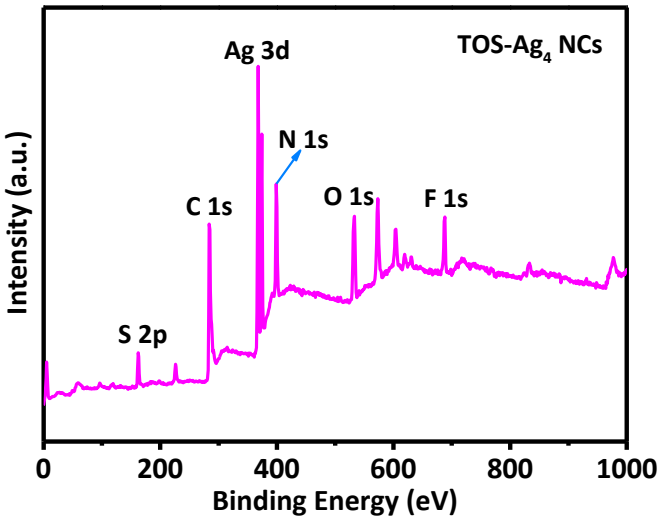

Figure S14. XPS full-scale spectrum of the as-prepared TOS-Ag_4 NCs.

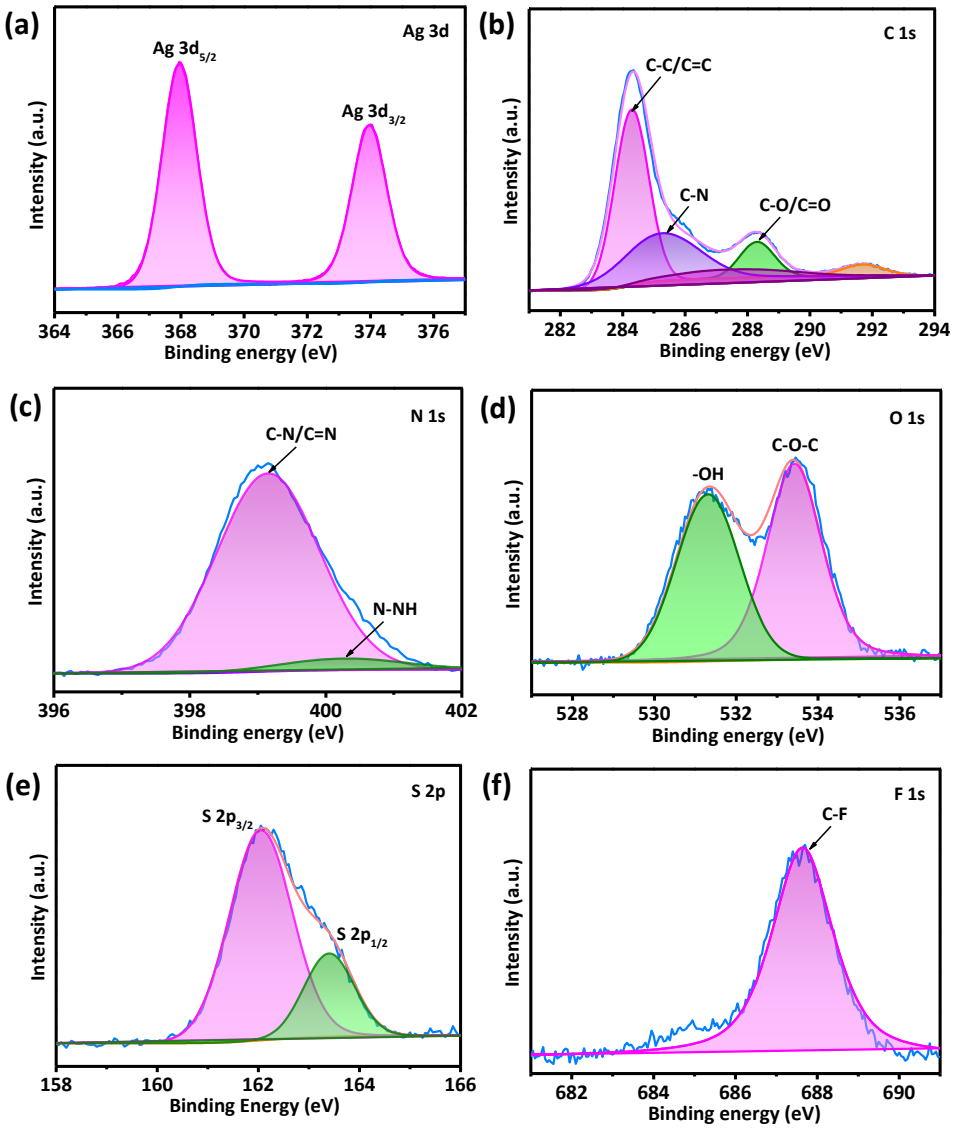

Figure S15. (a) Ag3d spectrum, (b) C1s spectrum, (c) N1s spectrum, (d) O1s spectrum, (e) S2p spectrum and (f) F1s spectrum of the as-prepared TOS-Ag_4 NCs.

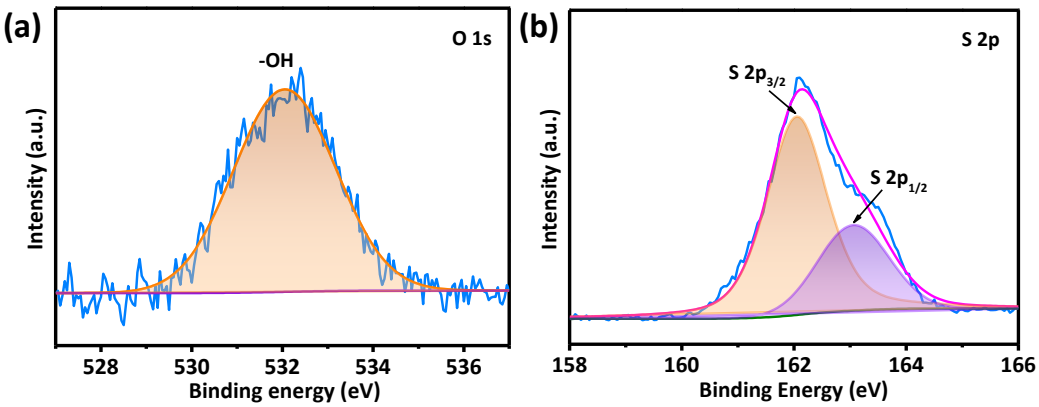

Figure S16. (a) O1s spectrum and (b) S2p spectrum of the as-prepared TNS-Ag_8 NCs.

4. SERS measurements of TOS-Ag_4 NCs and TNS-Ag_8 NCs

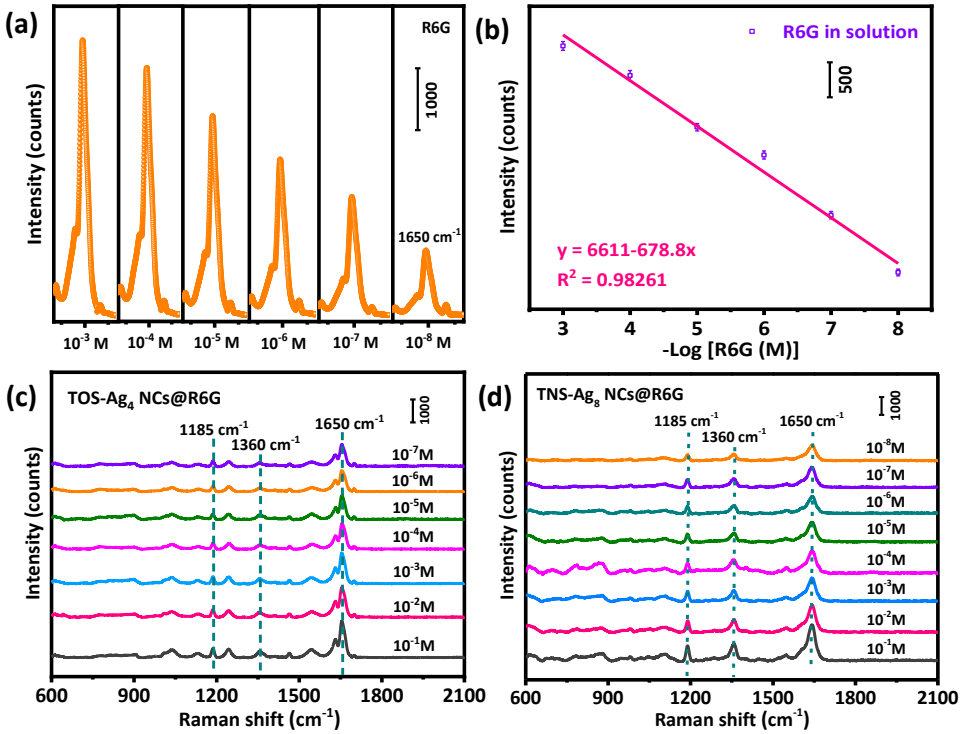

Figure S17. (a) The SERS spectra of R6G at 1650 cm^{-1} were acquired at varied concentrations. (b) Plots of the SERS peak intensity of R6G at 1650 cm^{-1} as a function of its concentration. The plot shows the standard linear relationship between the SERS signals intensity at 1650 cm^{-1} with the logarithm of concentrations of R6G. (c) Raman spectra of R6G with the concentration from 10^{-1} to 10^{-7} M on TOS-Ag_4 NCs. (d) Raman spectra of R6G with the concentration from 10^{-1} to 10^{-8} M on TNS-Ag_8 NCs. The limit of detection of R6G was determined by comparing the SERS signals intensity at 1650 cm^{-1} with a standard curve.

Table S2. Performance comparison of TOS-Ag_4 NCs and TNS-Ag_8 NCs SERS substrates towards the detection of R6G.

SERS Substrate	Analyte	Limit of Detection	Enhancement Factor	RSD (%)
TOS-Ag_4 NCs	R6G	10^{-7} M	8.3×10^4	4.67
TNS-Ag_8 NCs	R6G	10^{-8} M	3.6×10^4	5.51

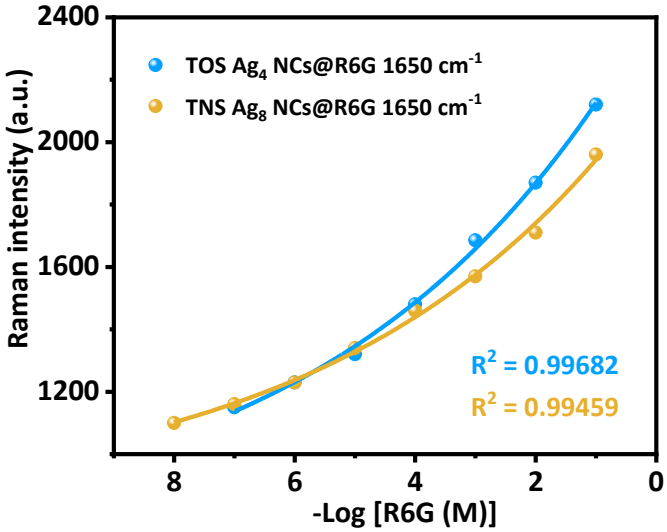

Figure S18. GuassAmp nonlinear curve fitting between R6G 1650 cm^{-1} peak intensities and logarithm of concentrations.

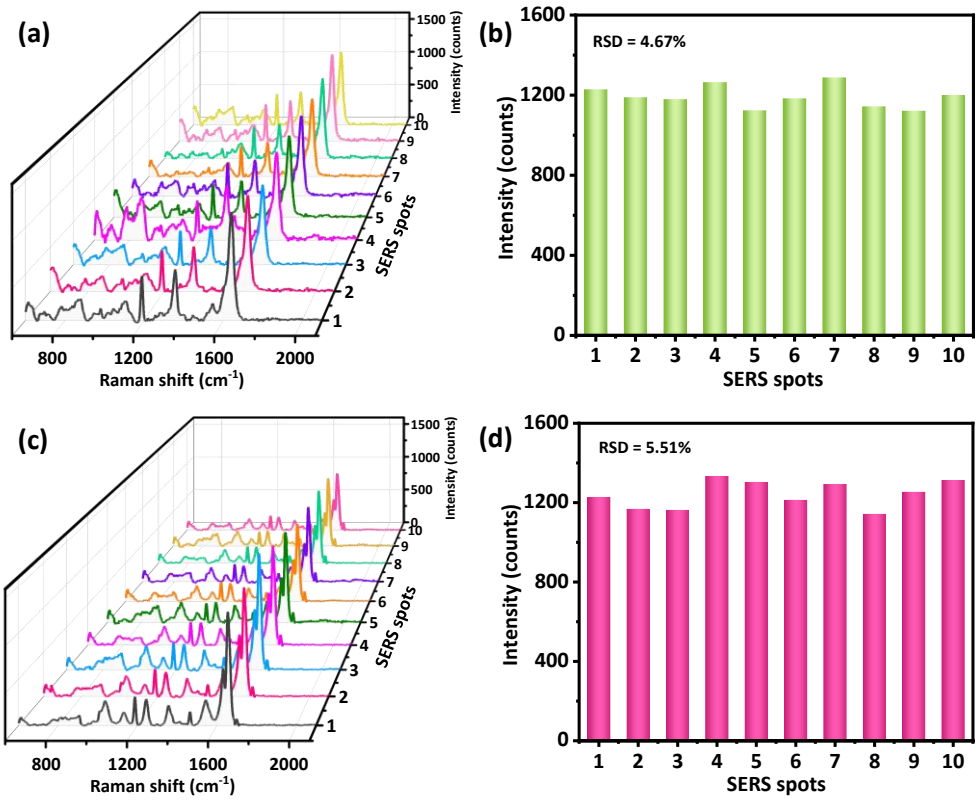

Figure S19. (a) SERS spectra of R6G recorded from 10 random points on TOS-Ag_4 NCs. (b) SERS intensity changed at 1650 cm^{-1}. (c) SERS spectra of R6G recorded from 10 random points on TNS-Ag_8 NCs. (d) SERS intensity changed at 1650 cm^{-1}. For the calculation of relative standard deviation (RSD) spot-to-spot on the SERS substrate, the SERS substrate was tested for sensing 10^{-6} R6G and 10 spectra were randomly collected from each sample and the average values were used for the RSD calculation.

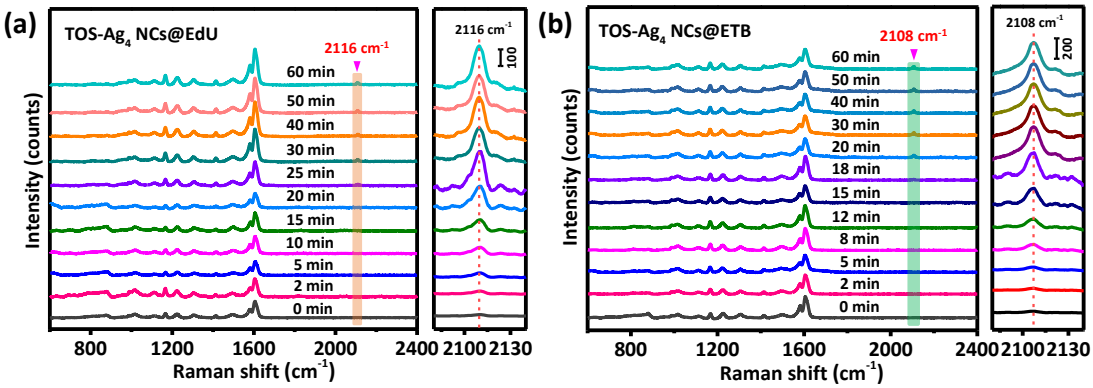

Figure S20. SERS spectra of TOS-Ag_4 NCs substrate taken at different times after its exposure to 10^{-3} M (a) EdU and (b) ETB. The right figure is an enlarged spectrum in the 2080-2140 cm^{-1} regions.

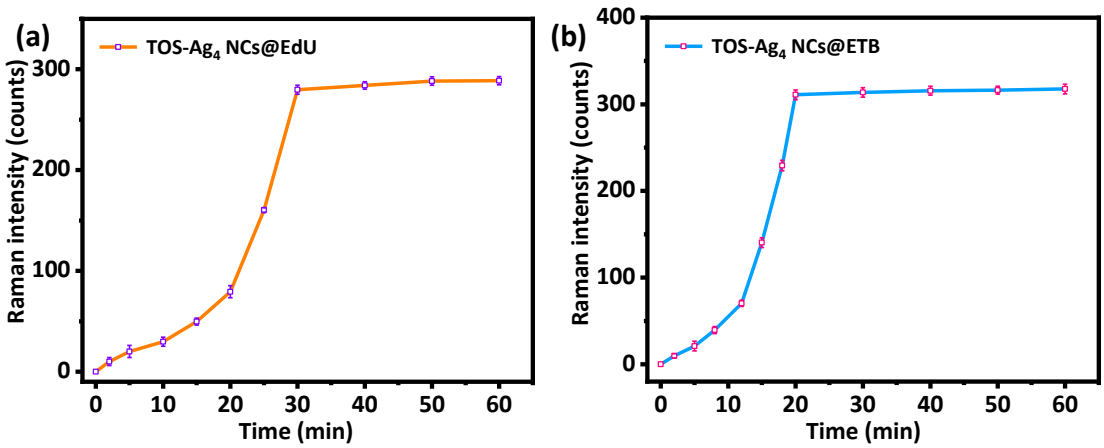

Figure S21. The time-dependent SERS intensities changes of (a) EdU (2116 cm^{-1}) and (b) ETB (2108 cm^{-1}) adsorb on TOS-Ag_4 NCs, respectively.

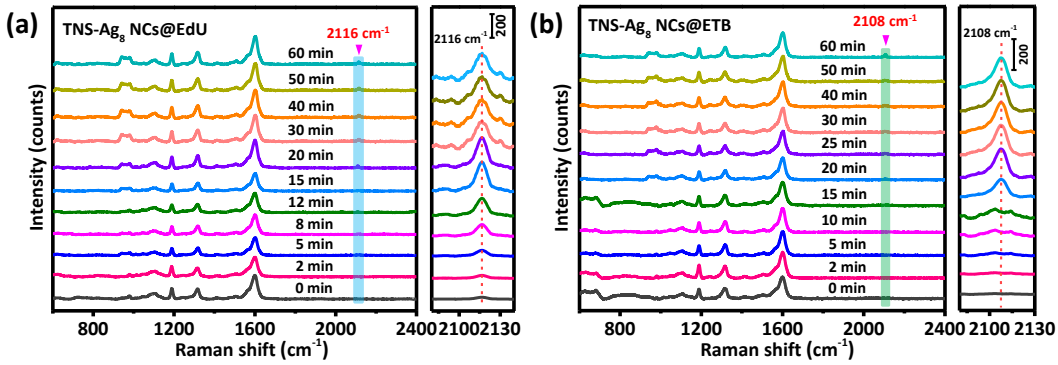

Figure S22. SERS spectra of TNS-Ag_8 NCs substrate taken at different times after its exposure to 10^{-3} M (a) EdU and (b) ETB. The right figure is an enlarged spectrum in the 2080-2140 cm^{-1} regions.

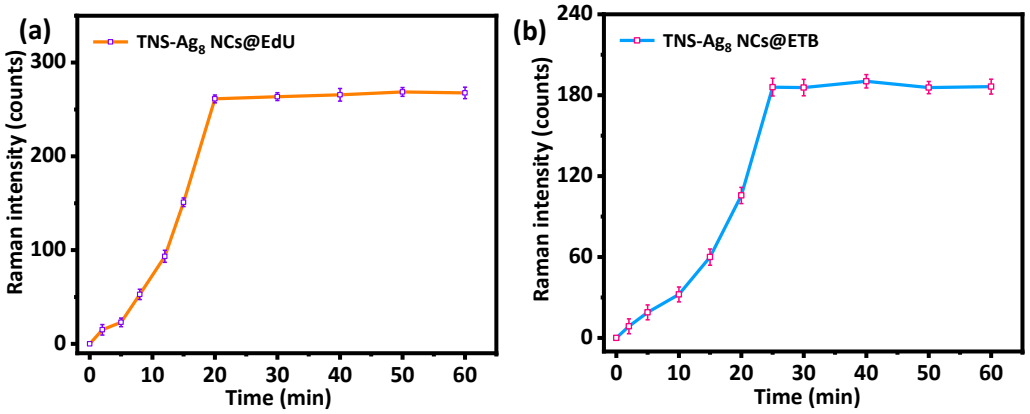

Figure S23. The time-dependent SERS intensities changes of (a) EdU (2116 cm^{-1}) and (b) ETB (2108 cm^{-1}) adsorb on TNS-Ag_8 NCs, respectively.

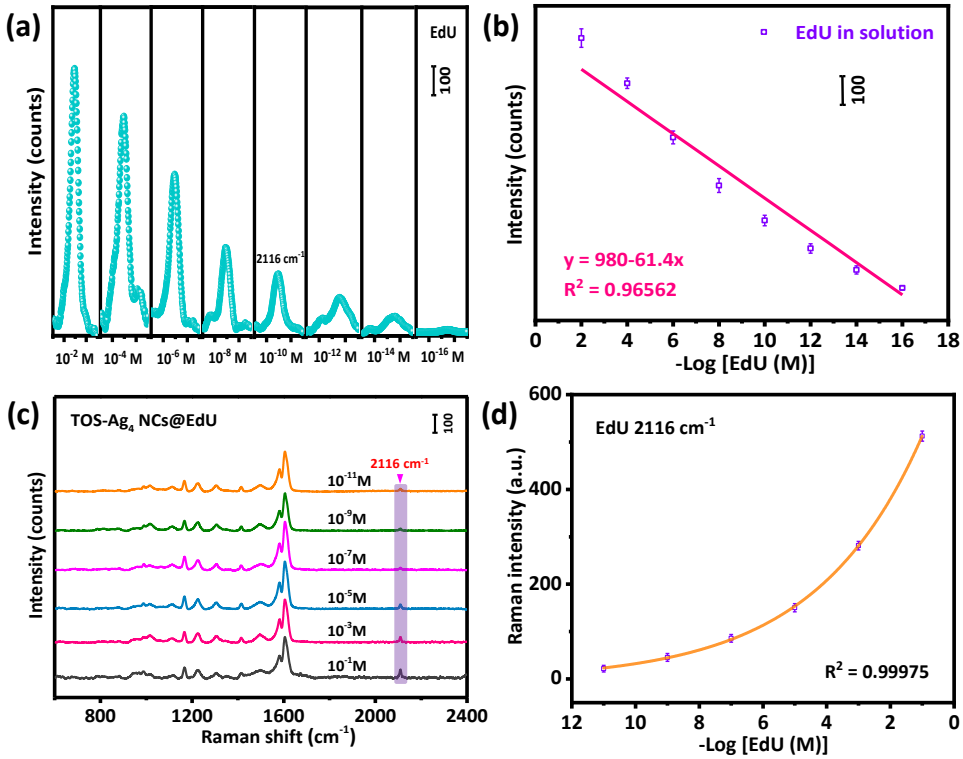

Figure S24. (a) The SERS spectra of EdU at 2108 cm^{-1} were acquired at varied concentrations. (b) Plots of the SERS peak intensity of EdU at 2108 cm^{-1} as a function of its concentration. The plot shows the standard linear relationship between the SERS signals intensity at 2116 cm^{-1} with the logarithm of concentrations of EdU. (c) Raman spectra of EdU with the concentration from 10^{-1} to 10^{-11} M on TOS-Ag_4 NCs. The limit of detection of ETB was determined by comparing the SERS signals intensity at 2116 cm^{-1} with a standard curve. (d) GuassAmp nonlinear curve fitting between EdU 2116 cm^{-1} peak intensities and logarithm of concentrations.

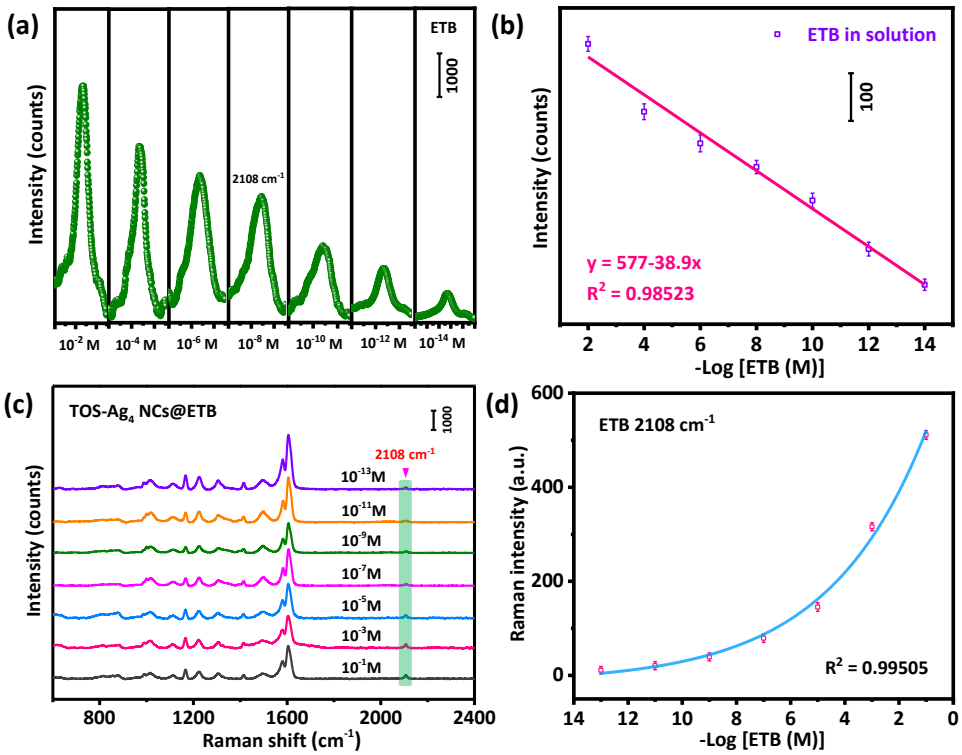

Figure S25. (a) The SERS spectra of ETB at 2108 cm^{-1} were acquired at varied concentrations. (b) Plots of the SERS peak intensity of ETB at 2108 cm^{-1} as a function of its concentration. The plot shows the standard linear relationship between the SERS signals intensity at 2108 cm^{-1} with the logarithm of concentrations of ETB. (c) Raman spectra of ETB with the concentration from 10^{-1} to 10^{-13} M on TOS-Ag_4 NCs. The limits of detection of ETB was determined by comparing the SERS signals intensity at 2108 cm^{-1} with a standard curve. (d) GuassAmp nonlinear curve fitting between ETB at 2108 cm^{-1} peak intensities and logarithm of concentrations.

Table S3. Performance comparison of TOS-Ag_4 NCs and TNS-Ag_8 NCs SERS substrates towards the detection of EdU and ETB.

SERS Substrate	Analyte	Limit of Detection	Enhancement Factor	RSD (%)
TOS-Ag_4 NCs	EdU	10^{-11} M	4.8×10^{6}	4.31
TOS-Ag_4 NCs	ETB	10^{-13} M	1.2×10^{5}	2.91
TNS-Ag_8 NCs	EdU	10^{-15} M	5.0×10^{7}	2.53
TNS-Ag_8 NCs	ETB	10^{-13} M	3.2×10^{6}	2.38

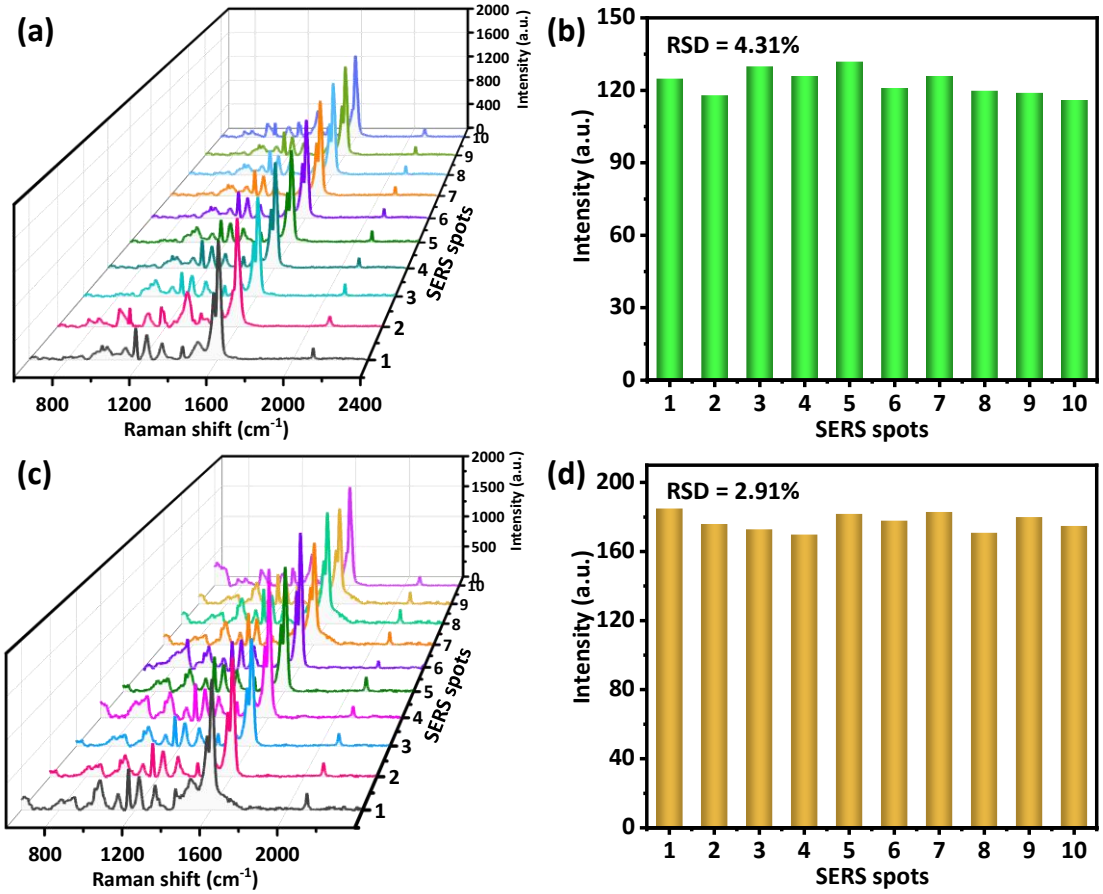

Figure S26. (a) SERS spectra of EdU (10^{-5} M) recorded from 10 random points on TOS-Ag_4 NCs. (b) SERS intensity changed at 2116 cm^{-1}. (c) SERS spectra of ETB (10^{-5} M) recorded from 10 random points on TOS-Ag_4 NCs. (d) SERS intensity changed at 2108 cm^{-1}.

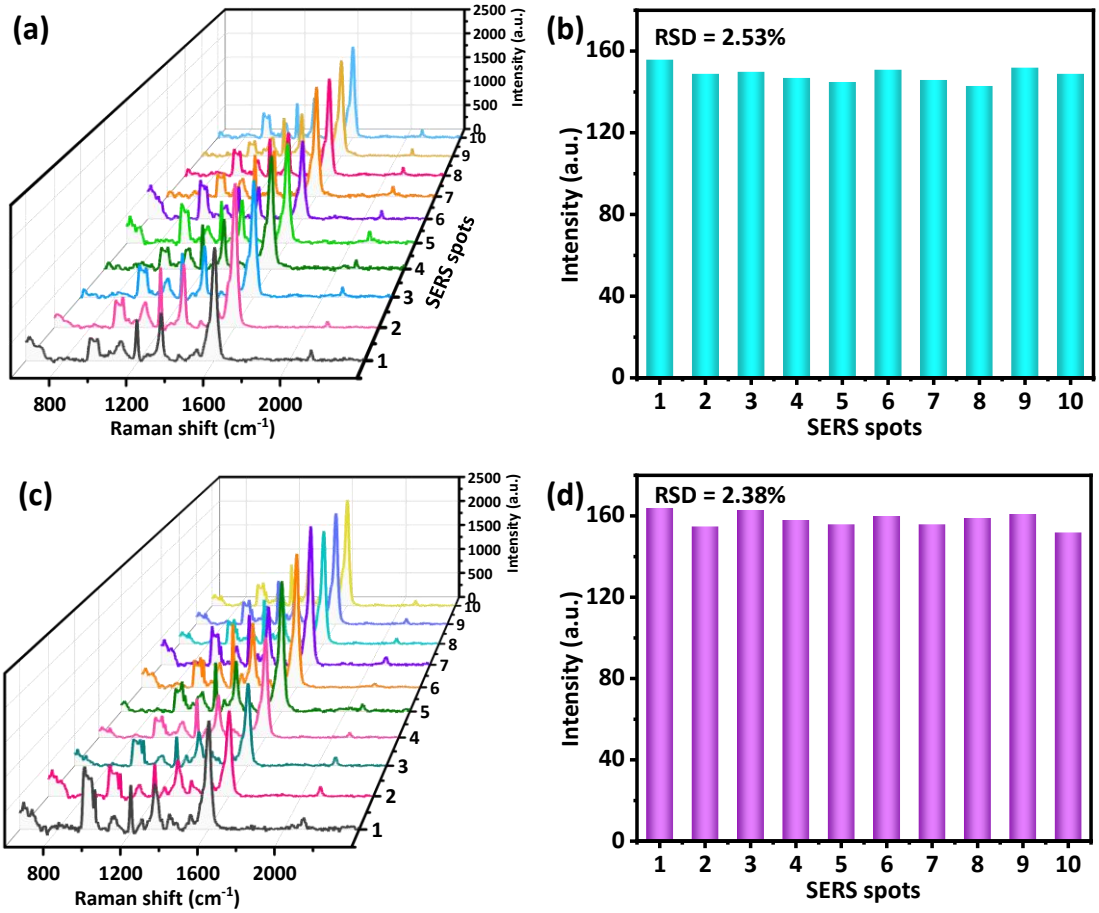

Figure S27. (a) SERS spectra of EdU (10^{-5}M) recorded from 10 random points on TNS-Ag_8 NCs. (b) SERS intensities changed at 2116 cm^{-1}. (c) SERS spectra of ETB (10^{-5} M) recorded from 10 random points on TNS-Ag_8 NCs. (d) SERS intensity changed at 2108 cm^{-1}.

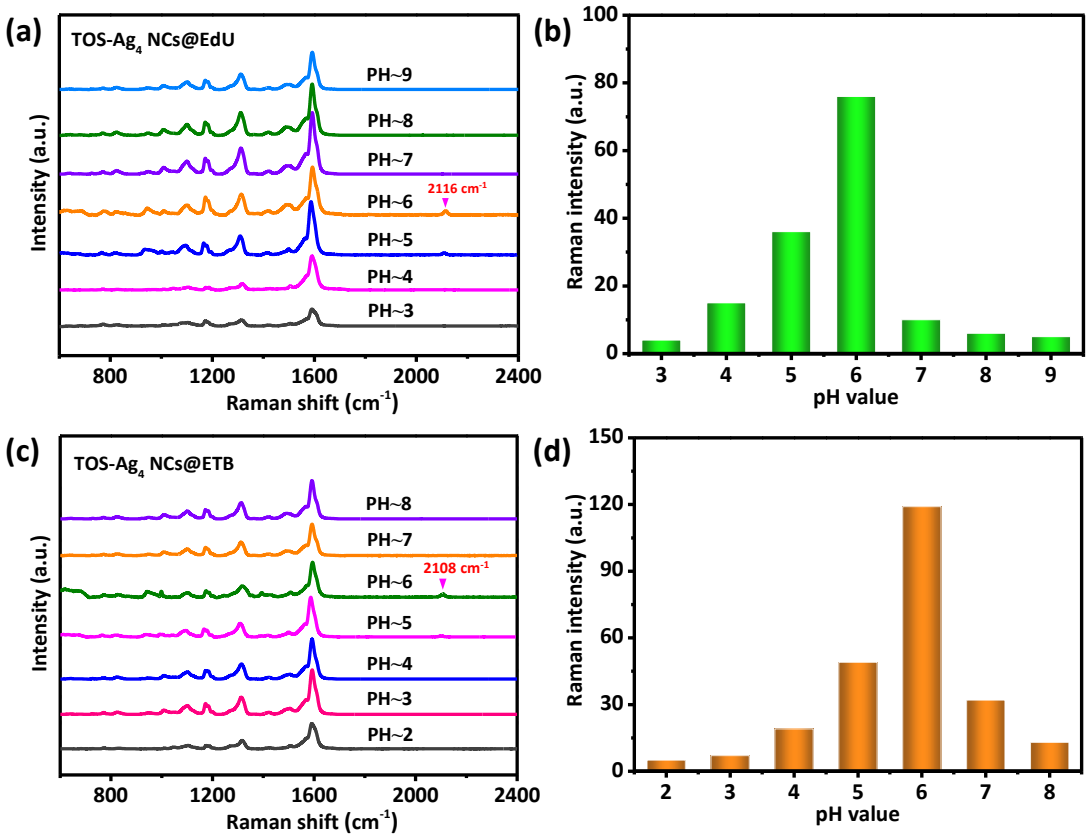

Figure S28. (a) SERS spectra of EdU (10^{-5} M) on TOS-Ag_4 NCs substrate at different pH values. (b) SERS intensity of the alkyne on-resonance bands (2116 cm^{-1}) of EdU on TOS-Ag_4 NCs at different pH values. (c) SERS spectra of ETB (10^{-5} M) on TOS-Ag_4 NCs substrate at different pH values. (d) SERS intensity of the alkyne on-resonance bands (2108 cm^{-1}) of ETB on TOS-Ag_4 NCs at different pH values.

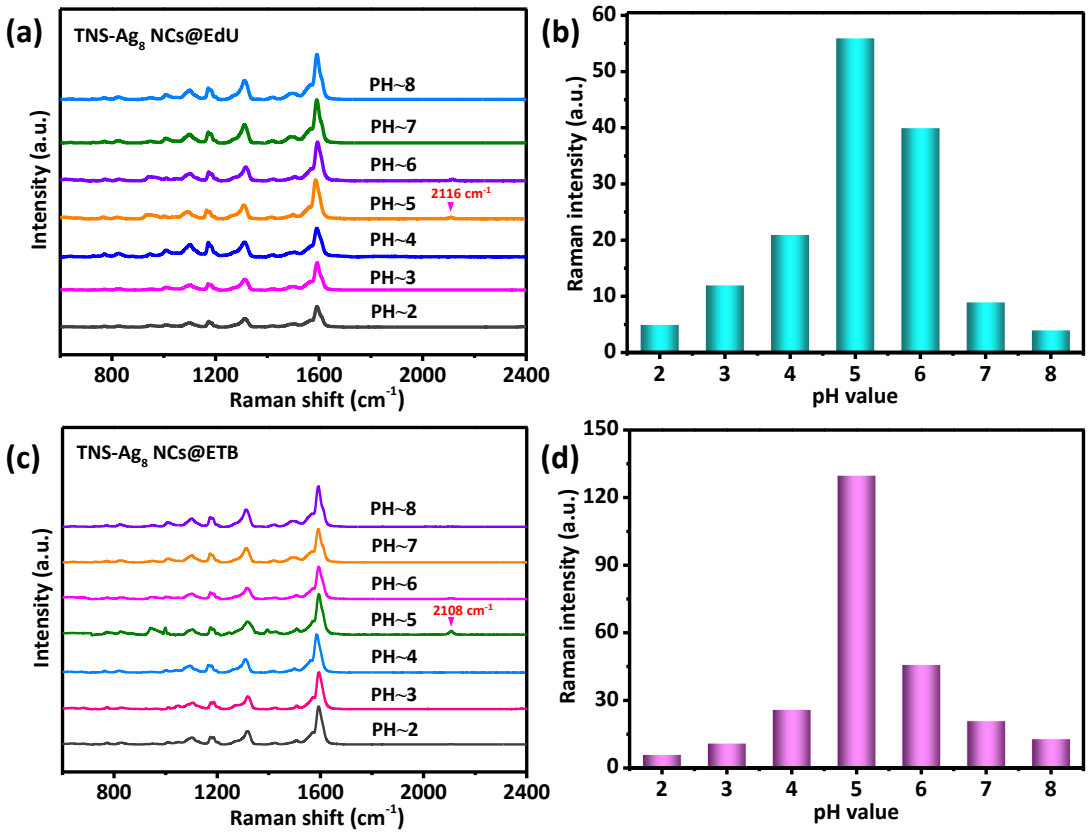

Figure S29. (a) SERS spectra of EdU (10^{-5} M) on TNS-Ag_8 NCs substrate at different pH values. (b) SERS intensity of the alkyne on-resonance bands (2116 cm^{-1}) of EdU on TNS-Ag_8 NCs at different pH values. (c) SERS spectra of ETB (10^{-5} M) on TNS-Ag_8 NCs substrate at different pH values. (d) SERS intensity of the alkyne on-resonance bands (2108 cm^{-1}) of ETB on TNS-Ag_8 NCs at different pH values.

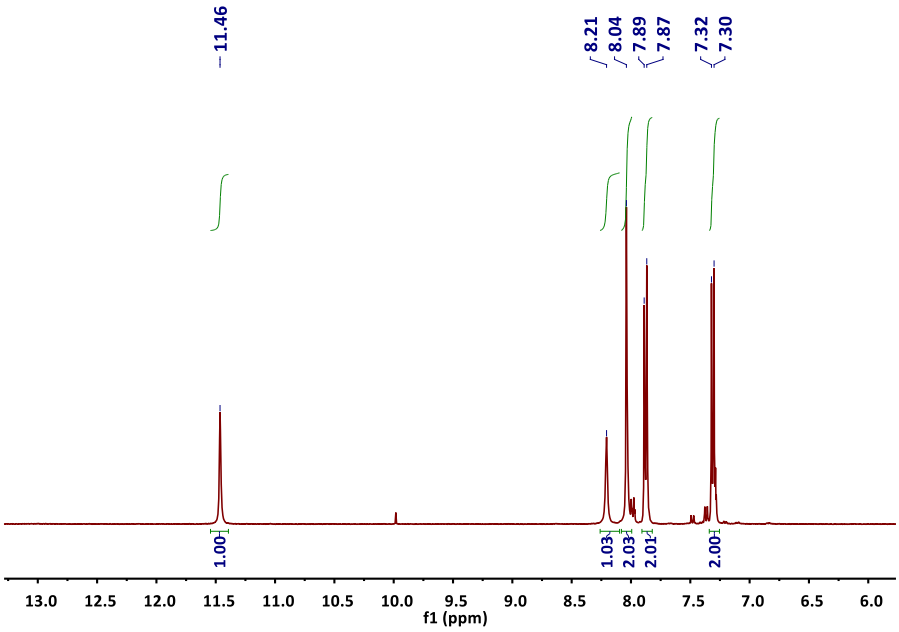

Figure S30. ^{1}H NMR (400 MHz, DMSO-d_6) spectrum of H_3L_1.

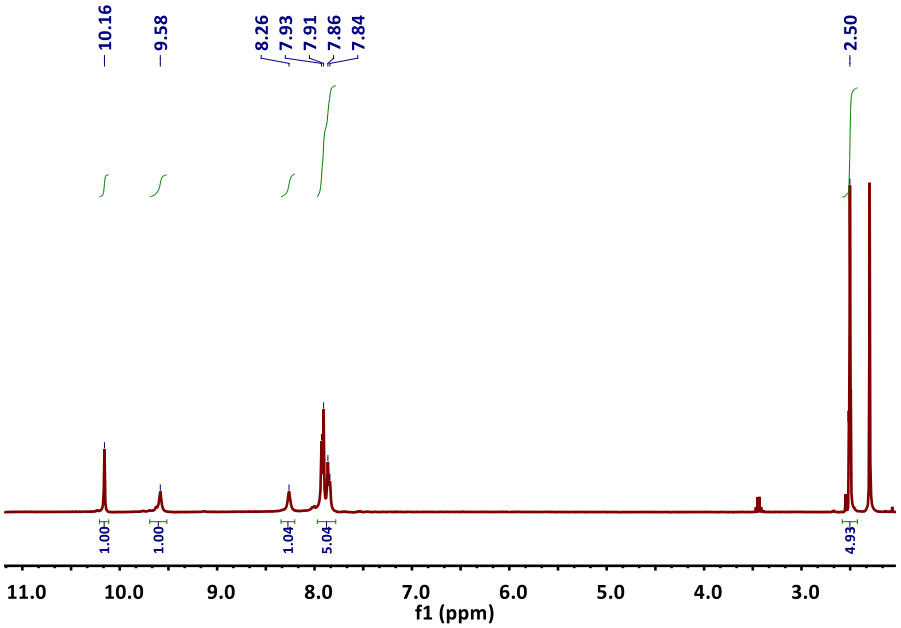

Figure S31. ^{1}H NMR (400 MHz, DMSO-d_6) spectrum of H_3L_2.

5. References

S1. J. A. Mikroyannidis, S. S. Sharma, Y. K. Vijay and G. D. Sharma, *ACS Appl. Mater. Interfaces*, 2010, **2**, 270-278.

S2. Z. D. Chang, X. Jing, C. He, X. Liu and C. Y. Duan, *ACS Catal.*, 2018, **8**, 1384-1391.

S3. W. L. Fu, S. J. Zhen and C. Z. Huang, *Analyst*, 2013, **138***,* 3075-3081.

S4. X. J. Liu, L. Y. Cao, W. Song, K. L. Ai and L. H. Lu, *ACS Appl. Mater. Interfaces*., 2011, **3***,* 2944-2952.